Article

Boron effect on microstructure, superplastic behavior, and mechanical properties of Ti-4Al-3Mo-1V alloy

Maria N. Postnikova[1], Anton D. Kotov[1]*, Andrey I. Bazlov[1], Ahmed O. Mosleh[2], Svetlana V. Medvedeva and Anastasia V. Mikhaylovskaya[1]

[1] Department of Physical Metallurgy of Non-Ferrous Metals, National University of Sciences and Technology "MISIS", 4 Leninskiy ave. 4, 119049 Moscow, Russia.; sitkina.m@misis.ru; bazlov@misis.ru; medvedeva71@list.ru; mihaylovskaya@misis.ru

[2] Department of Mechanical Engineering, Faculty of Engineering at Shoubra, Benha University, 11629 Cairo, Egypt; ahmed.omar@feng.bu.edu.eg

* Correspondence: kotov@misis.ru; Tel.: +7-495-955-01-34

Abstract: The microstructure evolution, superplasticity, and room temperature mechanical properties of Ti-4%Al-1%V-3%Mo alloys modified with 0.01-2 wt.% boron were investigated. Increasing the boron content from 0 to 0.1 wt.% effectively refined prior β-grains, reducing a mean grain size from ~700 μm to ~210 μm. Whiskers of the TiB phase with a size in a range of 0.7-2.9 μm were observed after solidification and thermomechanical processing. Alloys with 0.01-0.1 wt.% boron exhibited similar superplastic elongations and strain rate sensitivity coefficient m of 0.4-0.5 at a strain rate of 1×10^{-3} s^{-1} and the elongation to failure decreased from 1000% at 875°C to 400-500% at 700°C. Along with this, the minor boron addition effectively decreased flow stress values, especially at 775 °C, that was explained by the acceleration of the recrystallization and globularization of the microstructure at the initial stage of deformation. Recrystallization-induced decrease in yield strength from 770 MPa to 680 MPa was observed with an increase in boron content from 0 to 0.1 wt.%. Heat treatment increased post-forming strength characteristics for the alloys with 0.01-0.1 wt.% boron by 90–140 MPa without ductility reduction. Alloys with 1-2 wt.% B demonstrated the opposite behavior. The grain refinement effect was not revealed, and prior β grain sizes were ~670-750 μm after solidification. Thermomechanical processing promoted the fragmentation of boride whiskers and the formation of near-spherical particles with a size of ~1 μm for the alloy with a eutectic concentration of 2 wt.% B. A high fraction of borides, ~5-11%, in the alloys with 1-2 wt.% B deteriorated the superplastic properties and drastically decreased ductility at room temperature. The alloy with 2 wt.% B demonstrated non-superplastic behavior and a low level of mechanical properties, meanwhile, the alloy with 1% boron exhibited high-temperature superplasticity at 875 °C with elongation of ~500%, and yield strength of 830 MPa, ultimate tensile strength of 1020 MPa at a room temperature after 100% of superplastic deformation.

Keywords: titanium alloys, superplasticity, TiB, ultrafine-grained structure, thermomechanical treatment, metal matrix composites

1. Introduction

Titanium alloys are widely used in aircraft, transport, medicine, and chemical industries due to their high specific strength and corrosion resistance. However, obtaining parts from titanium alloys by traditional methods at low temperatures is a difficult and energy-consuming process due to their high strength, low elasticity modulus, and high sensitivity to processing parameters [1]. Superplastic forming (SPF) is an alternative to traditional forming methods by producing parts of complex geometry in one forming operation at a low gas pressure and with high dimensional accuracy [2,3]. The superplastic behavior of titanium alloys depends on the grain size and shape and α/β phase ratio [4,5]. Control of the grain structure and its evolution are required to ensure excellent superplasticity. Grain

 doi:10.20944/preprints202304.0194.v1

size control is an important issue from the step of solidification to thermomechanical processing and superplastic deformation.

Alloying with 0.05-0.2 wt.% B (boron) improves the processing and mechanical properties of titanium-based alloys [6–9]. Boron is low soluble (up to 0.02 wt.% [10,11]) in titanium and it forms fine particles of the TiB phase [12–14]. The TiB particles solidify at eutectic transformation and exhibit the elongated shape of "whiskers" [15,16]. Trace addition of boron in titanium and titanium-based alloys provides a strong grain refinement effect during solidification [8,9,17]. The grain refinement mechanism is related to the TiB phase solidification [18–22]. According to the Ti-B phase diagram, hypoeutectic β-Ti grains solidify first and the eutectic-originated TiB phase could not stimulate β-Ti phase nucleation in the liquid phase at the B content below ~2% [22]. Larson presumes [23] that the borides can act as inoculants, i.e. ingot re-melts several times and eutectic-originated borides do not dissolve during the re-melting process. The most acceptable refinement mechanism is related to a refinement of dendrite arm spacing due to B atomic segregations at the front of solidification and constitutional supercooling effect [24]. The Zener pinning effect of TiB particles in a solid state is also possible [25]. A trace amount of 0.02 wt.% B refines grains for Ti–6Al–4V alloy [26,27] and the effect intensifies up to 0.1 wt.% B [24]. The grain size for alloys with 0.1 wt.% B is similar for 0.4 wt.% B, therefore, the 0.1 wt% considers the most effective [24].

For wrought alloys, boron provides globularization of the microstructure during heat and thermomechanical treatments. The proposed mechanism is stimulation of the α phase nucleation near TiB particles [28,29]. Authors of [16] observe boron atomic segregations at the α/β interfaces and reasonably assume the 'boron solute pinning mechanism' for α-phase colonies.

The TiB phase has an equivalent density to titanium but five times greater strength [30]. Notably, the TiB phase is stable over a wide temperature range [30]. These particles are efficient reinforces at a considerable volume fraction [31]. An increase in boron content provides the natural composite structure of the Ti-based alloys reinforced with in-situ precipitated TiB whiskers. High-boron alloys have significant practical importance and their microstructure and properties have been studied but scarcely [9,30,32].

Thus, minor boron refines the grain structure in the as-cast state as well as after thermo-mechanical processing and increases the homogeneity of the microstructure in the ingots and thermomechanically treated products [9,28,33–35]. The effectiveness of a trace amount of boron for grain refinement of unalloyed Ti and several Ti-based alloys is confirmed. The B effect depends on the alloy composition, residual elements [23]and treatment parameters, and further investigations for the alloys with different boron content and different chemical compositions are required to convince the industry of the effectiveness of B alloying.

A conventional Ti-4Al-1V-3Mo alloy is widely applied due to its high strength, excellent corrosion resistance good creep resistance. The alloy exhibits superplasticity in the temperature range of 825-875 °C similar to Ti-6Al-4V [36,37]. In contrast to the widely used Ti-6Al-4V alloy, the deformation behavior of Ti-4Al-1V-3Mo alloy is characterized by strain softening, owing to dynamic recrystallization, that complicated superplastic forming [38]. Due to grain refinement, a trace addition of 0.1%B improves superplastic properties and increases the superplastic formability of the Ti-6Al-4V alloy [28]. The complex alloying with B and Fe improves superplasticity and decreases superplastic deformation temperature for Ti-4Al-3Mo-1V alloy but the effect of B for complexly alloyed materials is not clear [39,40]. This work studies the influence of boron in a range of 0.01-2 wt.% on the microstructure, superplasticity, and mechanical properties at room temperature of the Ti-4Al-3Mo-1V.

2. Materials and Methods

The boron-free reference Ti-Al-V-Mo alloy and five alloys with boron additions in a range of 0.01-2 wt.% were investigated (Table 1). The ingots were processed by argon arc melting in a laboratory vacuum furnace Arc Melter ARC200 (ARCAST Company, Oxford,

Preprints (www.preprints.org) | NOT PEER-REVIEWED | Posted: 11 April 2023 doi:10.20944/preprints202304.0194.v1

MS, USA). The concentrations of Al, Mo, and V alloying elements in the alloys were similar. Titanium (>99.9 wt.%), aluminum (>99.99 wt.%), vanadium (>99.9 wt.%), boron (>99.99 wt.%), and the Ti – 50 wt.% Mo master alloy were used to prepare the alloys. The ~100 g ingots were re-melted five times to ensure a homogeneous alloy composition and cast into a copper water-cooled mold with an internal size of 50 × 40 × 10 mm^3. The ingots were subjected to homogenization annealing in finance with a vacuum atmosphere at 800 °C for 1 hour and subsequently heated to the β-field and quenched with water.

Table 1. Chemical composition of the investigated alloys (wt.%).

Alloy	Al	Mo	V	B	Ti
0B	4.2	3.0	1.1	-	Bal.
0.01B	4.1	3.2	1.0	0.01	Bal.
0.05B	4.1	2.9	0.9	0.05	Bal.
0.1B	3.9	3.1	1.1	0.1	Bal.
1B	4.2	3.0	1.0	1	Bal.
2B	4.3	3.1	1.1	2	Bal.

Quenched ingots of the 0B, 0.01B, 0.05B, and 0.1B alloys were hot-rolled with a total reduction of 90% at a temperature of 750 ± 10 °C. A low ductility did not allow to process of the high-boron alloys at 750 ± 10 °C. Ingots of the 1B and 2B alloys (with 1-2% B) were successfully rolled at a higher temperature of 900 ± 10 °C. The sheets were treated in Kroll's reagent (92% H2O + 3% HF + 5% HNO3) for 20-30 min to remove the α-phase layer from the surface. The final thickness of the hot-rolled sheets was 1.0 ± 0.1 mm.

The as-cast grain structure of the alloys was analyzed using a Neophot-30 optical (light) microscope (LM) with polarized light. To analyze the phase composition and grain size of the thermomechanical treated alloys, a Vega 3-LMH scanning electron microscope (SEM) (Tescan Brno s.r.o., Kohoutovice, Czech Republic) equipped with the EDS X-MAX 80 energy dispersive spectrometer (Oxford Instruments plc, Abingdon, UK) was used. The grain and sub-grain structure of the thermomechanical processed alloys was also analyzed with backscattered electron diffraction (EBSD) technique using HKL NordlysMax EBSD detector (Oxford Instruments plc, Abingdon, UK). The scanning area was 50×50 μm^2 at a scanning step was 0.15 μm. Samples for microstructural analysis were prepared by mechanical grinding and polishing on a CHEM MD cloth in a solution (silicon oxide suspension 50 ml, H_2O_2(30%) 10 ml, and Kroll reagent 5 ml) on a Struers LaboPol-5 (Struers APS, Ballerup, Denmark). To identify grain structure in an as-cast state, the samples were etched with Weck's reagent (H_2O 100 ml, ethanol 50 ml, ammonium biflouride NH4FHF 2 g).

X-ray phase analysis of the alloys was performed using a D8 ADVANCE X-ray diffractometer (Bruker, Billerica, MA, USA) in a CuKα radiation. The β-transus temperature was determined by differential thermal analysis (DTA) on Setaram LabSys (SETARAM Instrumentation, Caluire, France) as the start temperature of the phase transformation $\beta \rightarrow (\alpha+\beta)$. The samples were heated to 1000 °C in an argon atmosphere and then cooled down to room temperature with a cooling rate of 5 K/c. To calculate the equilibrium β-transus temperature for the studied alloys a Thermo-Calc (Thermo-Calc Software, Stockholm, Sweden) software and a TTTI3 database were used.

The superplastic deformation behavior was characterized by uniaxial tension tests at a constant rate and a step-by-step decrease in the strain rate at temperatures of 875 °C, 775 °C and 700 °C on a Walter Bai LFM-100 (Walter + Bai AG, Löhningen, Switzerland) universal testing machine in a furnace with an argon atmosphere. Samples with the gauge section size dimensions of 14×6×1 mm^3 were cut parallel to the rolling direction and annealed for 30 min at the superplastic deformation temperatures before testing.

The mechanical properties of the alloys at room temperature were determined on a Zwick Z250 testing machine after 100% deformation at a temperature of 875 °C with a

Preprints (www.preprints.org) | NOT PEER-REVIEWED | Posted: 11 April 2023 doi:10.20944/preprints202304.0194.v1

constant strain rate of 1 × 10^{-3} s^{-1} on samples with a gauge section size of 6×0.8×25 mm^3. Three samples per alloy were tested.

3. Results

3.1. Phase composition analysis

The boron content for the studied alloys was chosen in a hypoeutectic concentration range for (0.01-1%)B and at the eutectic point for 2%B according to the data of the polythermal cross-section of the Ti-4Al-3Mo-1V-B phase diagram (nominal composition) simulated with Thermo Calc (Figure 1a). XRD phase analysis for the alloys with trace boron addition of below 0.1 % and boron-free alloy identified the α and β phases. Due to a high boron content in the 1B and 2B alloys, the clear peaks of the TiB phase were revealed. The peaks of low intensity attributed to titanium boride were found for the alloy with 0.1%B and this phase did not observe in the alloys with 0.01-0.05%B.

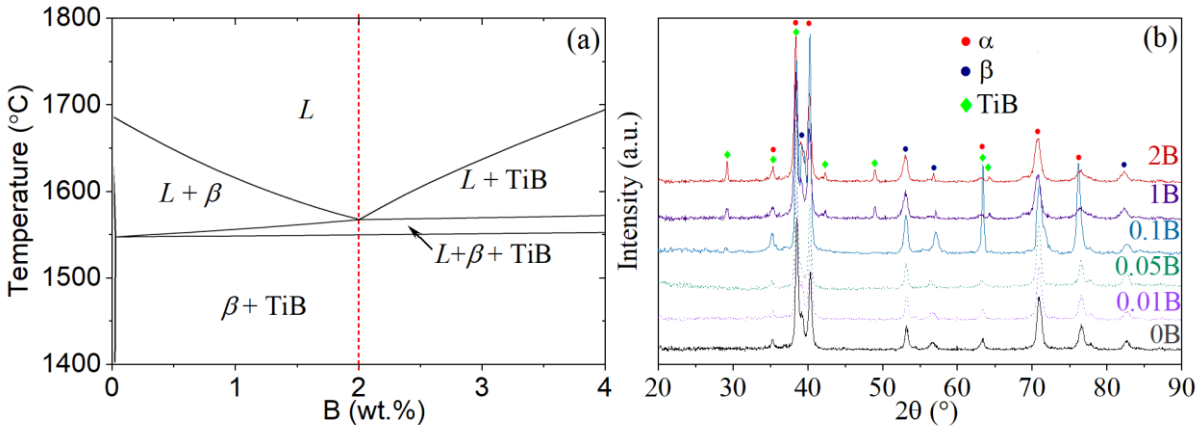

Figure 1. (a) Polythermal section of the Ti–4Al–3Mo–1V-B diagram (Thermo-Calc) and **(b)** XRD patterns for the alloys studied.

3.2. Analysis of the microstructure after solidification, thermomechanical treatment, and post-deformation annealing

The grain structure of the alloys in the as-cast state is shown in Figure 2. The addition of a trace amount of 0.01%B resulted in a decrease in the size of the primary β phase grains from 700±70 μm to 490±40 μm (Table 2). An increase of the boron content to 0.1% led to a significant decrease in grain size to 210±20 μm (Table 2). Surprisingly, for the alloys with a high boron content of 1-2% the average grain size was 710±50 μm, i.e., the value was similar to the boron-free alloy.

Preprints (www.preprints.org) | NOT PEER-REVIEWED | Posted: 11 April 2023 doi:10.20944/preprints202304.0194.v1

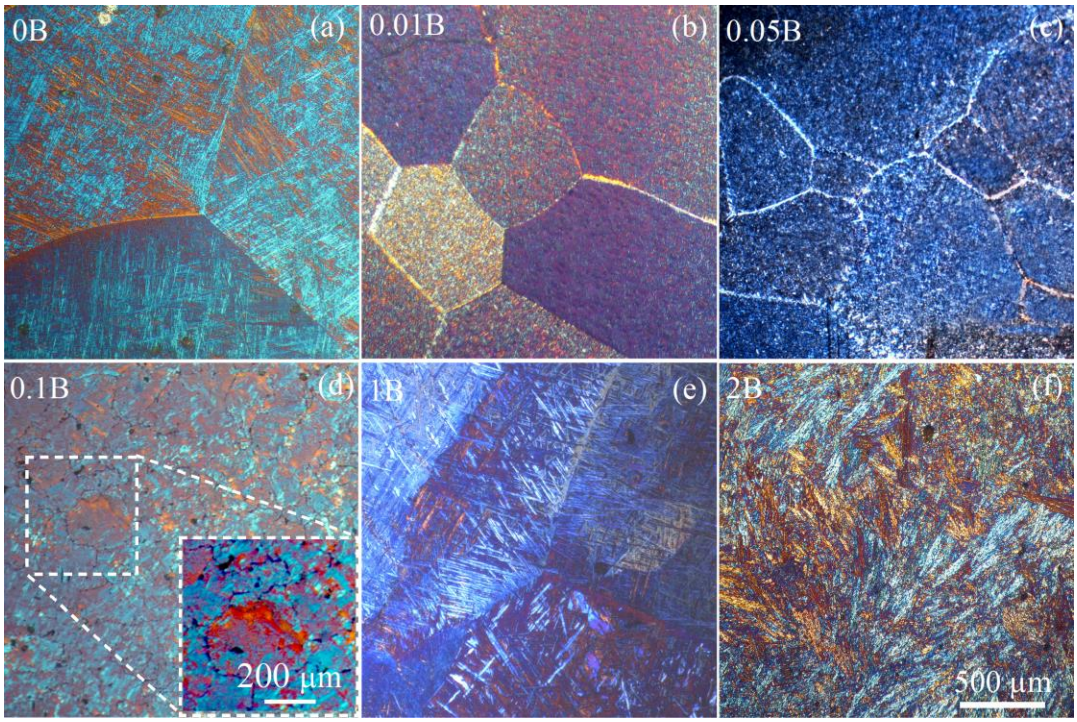

Figure 2. As-cast microstructure of the **(a)** 0B, **(b)** 0.01B, **(c)** 0.05B, **(d)** 0.1B, **(e)** 1B, and **(f)** 2B alloys.

SEM analysis of the alloys identified the matrix of the transformed prior β-grains and dark particles for all B-containing alloys after solidification (Figure 3). The EDS analysis revealed an increased boron content for the dark particles that indicated the TiB phase (Figure 4).

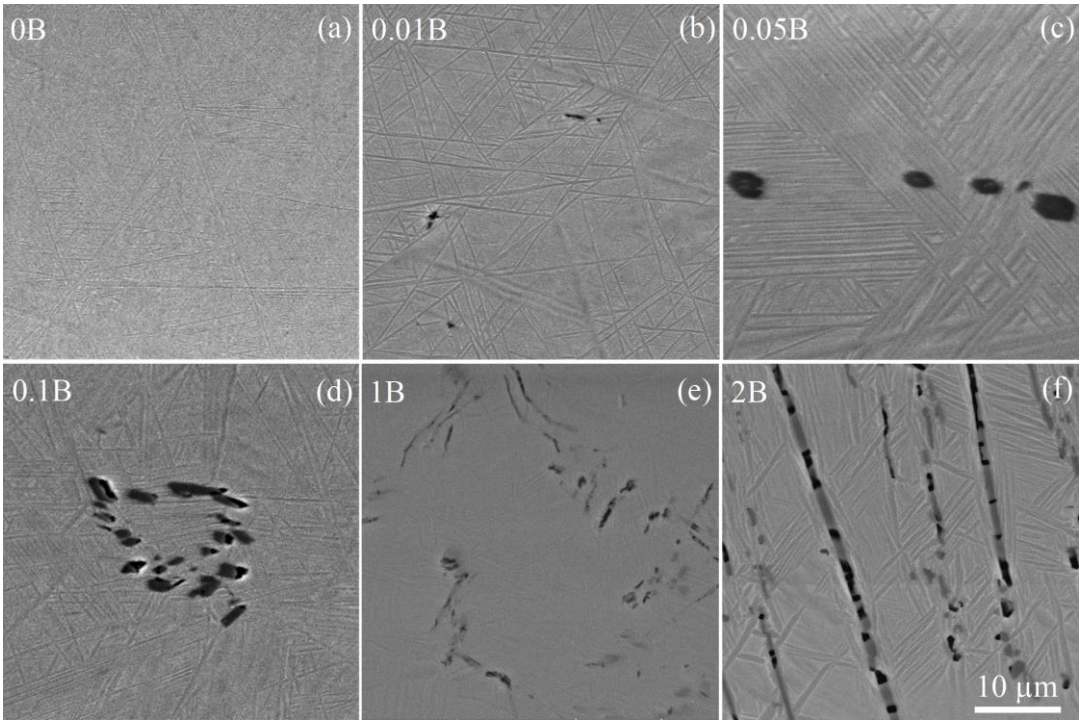

Figure 3. As-cast SEM images of the **(a)** 0B, **(b)** 0.01B, **(c)** 0.05B, **(d)** 0.1B, **(e)** 1B, and **(f)** 2B alloys.

The volume fraction of the TiB phase increased from 0.1 to 1.1% with an increase in boron content from 0.01 to 0.1%. Rarely distributed fine TiB particles were found in the 0.01B alloy, even at 0.01%B (Figure 3b). The individual TiB particles and their agglomerations were observed in the alloys with 0.05-0.1%B. The volume fraction of TiB particles

Preprints (www.preprints.org) | NOT PEER-REVIEWED | Posted: 11 April 2023 doi:10.20944/preprints202304.0194.v1

was 5.0 and 10.8% for high-boron alloys with 1 and 2%B, respectively (Table 2). The TiB particles were uniformly distributed in the matrix of the alloy with 2%B corresponding to eutectic composition (Figure 3f). The borides' morphology varied from compact polyhedral inclusions to elongated whiskers. For the 1B and 2B alloys, the TiB particles after solidification exhibited an elongated shape with a longitudinal size up to 9 μm, and finer and more compact-shaped borides were observed for the alloys with a low boron content of 0.01-0.1%. An average particle size increased from 0.7 to 2.5 μm with an increase in boron content from 0.01 to 0.1-1% and insignificantly grown to 2.9 μm for 2% B.

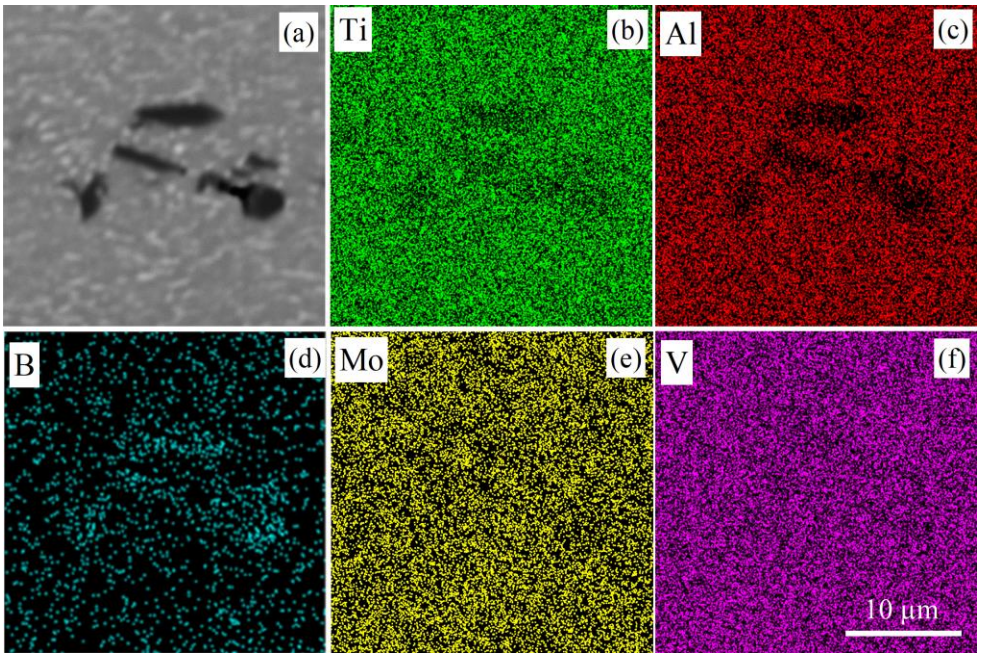

Figure 4. (a) SEM images and **(b-f)** EDS SEM maps of the hot-rolled 0.1B alloy.

Table 2. Microstructure parameters of the investigated alloys after solidification.

Alloy	TiB size (μm)	TiB volume fraction (%)	Grain size (μm)
0B	-		700±70
0.01B	0.7±0.2	0.1	490±40
0.05B	1.4±0.3	0.2	410±30
0.1B	2.5±0.4	1.1	210±20
1B	2.5±0.5	5.0	670±50
2B	2.9±0.5	10.8	750±80

The microstructure of the alloys studied after thermomechanical treatment was characterized by elongated grains of the α and β phases. The mean transverse sizes of both phases were similar for the studied alloys, the α-phase grains were in a range of 0.9–1.2 μm and the β-phase grains were in range of 0.5–0.8 μm (Figure 5, Table 3). The main difference between the microstructures of the rolled alloys was in the size and volume fraction of TiB particles (Table 3). Particles of the TiB phase in alloys with 0.1–1%B exhibited an elongated shape with a length ($L_{\parallel}$) of 2.1-3.1 μm and width ($L_{\perp}$) of 0.6–0.7 μm and a low aspect ratio ($L_{\perp}/L_{\parallel}$) of 0.2–0.3. In contrast, the morphology of TiB particles in the eutectic 2B alloy was characterized by a near-spherical shape with an aspect ratio ($L_{\perp}/L_{\parallel}$) equal to 1 and an average size of 1.0 μm.

Preprints (www.preprints.org) | NOT PEER-REVIEWED | Posted: 11 April 2023 doi:10.20944/preprints202304.0194.v1

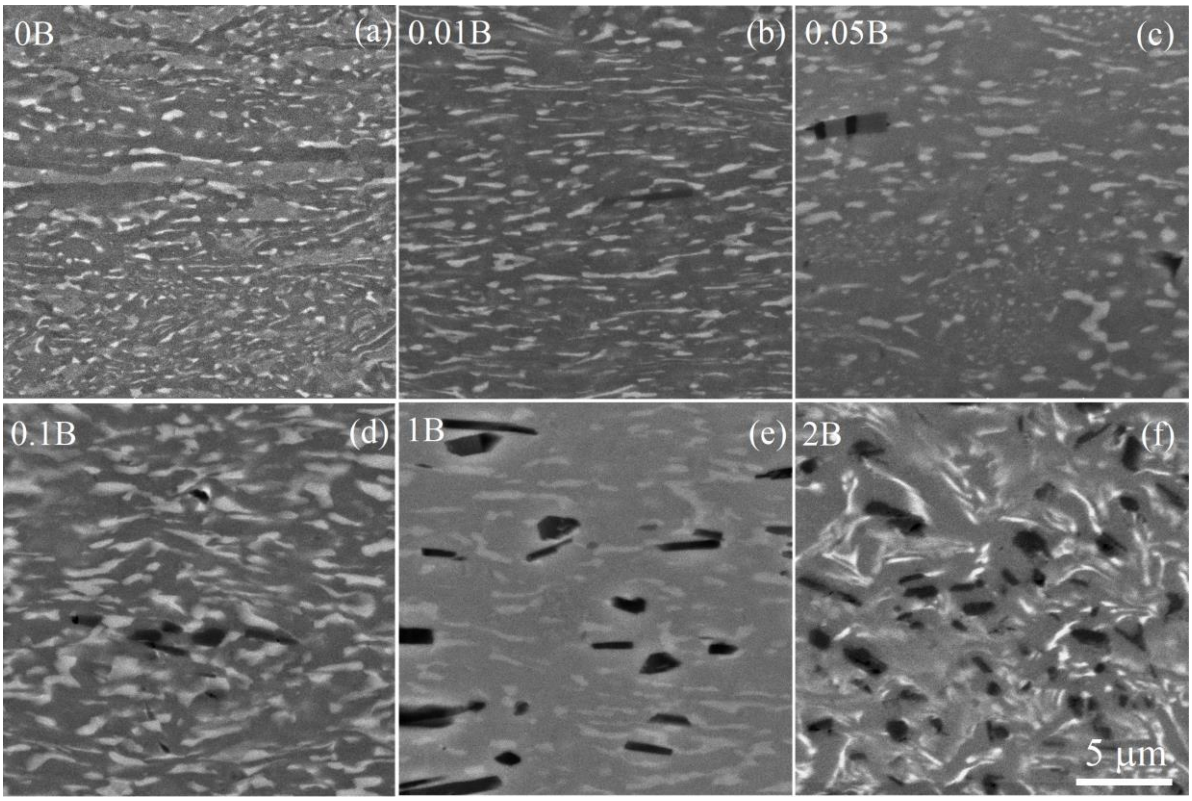

Figure 5. SEM images of the hot-rolled **(a)** 0B, **(b)** 0.01B, **(c)** 0.05B, **(d)** 0.1B, **(e)** 1B, and **(f)** 2B alloys.

Table 3. Microstructure parameters of the investigated alloys after thermomechanical processing.

Alloy	TiB size (μm)		$L_\perp/L_\parallel$	Grain size (μm)		Volume fraction (%)		
	$L_\parallel$	$L_\perp$		α	β	α	β	TiB
0B*	-	-	-	1.0±0.2	0.5±0.1	80	20	-
0.01B*	2.1±0.3	0.6±0.1	0.3	1.0±0.1	0.7±0.1	82	18	0.2
0.05B*	2.2±0.4	0.7±0.1	0.3	1.0±0.1	0.7±0.1	80	20	0.3
0.1B*	2.8±0.2	0.7±0.3	0.2	0.9±0.1	0.6±0.1	78	18	1.1
1B**	3.1±0.9	0.7±0.2	0.2	1.2±0.1	0.8±0.1	76	19	5.2
2B**	1.0±0.2	1.0±0.1	1.0	1.0±0.1	0.6±0.1	70	20	10.5

* - hot-rolled at 750 °C, ** - hot-rolled at 900 °C.

Annealing at 875 °C for 30 minutes, which simulated the microstructure before the onset of superplastic deformation, did not influence on the morphology and fraction of borides. Meanwhile, the microstructure of boron-free and boron-bearing alloys were different (Figure 6). The microstructure of the B-free alloy was inhomogeneous. A high non-recrystallized fraction with elongated grains of both α and β phases was observed (Figure 6a-c). The alloy with 0.1%B was characterized by a globular equiaxed microstructure (Figure 6d-f). EBSD analysis revealed a significant difference in the grain/subgrain structures of 0B and 0.1B alloys (Figure 7). A fraction of low-angle grain boundaries was 40% (Figure 7a,b), a mean KAM angle was 0.82° (Figure 7c,d) and a substructured volume (Figure 7e) was dominated for B-free alloy. The smaller LAGBs fraction of 22% (Figure 7f,g), and smaller mean KAM angle of 0.46° (Figure 7h, i) were revealed, and recrystallized volume dominated for 0.1B alloy (Figure 7j). The mean grain/subgrain sizes for the α phase with HCP structure (including α and transformed β) were 1.0 μm/0.6 μm for 0B and 1.7 μm/1.1 μm for 0.1B alloy.

Preprints (www.preprints.org) | NOT PEER-REVIEWED | Posted: 11 April 2023 doi:10.20944/preprints202304.0194.v1

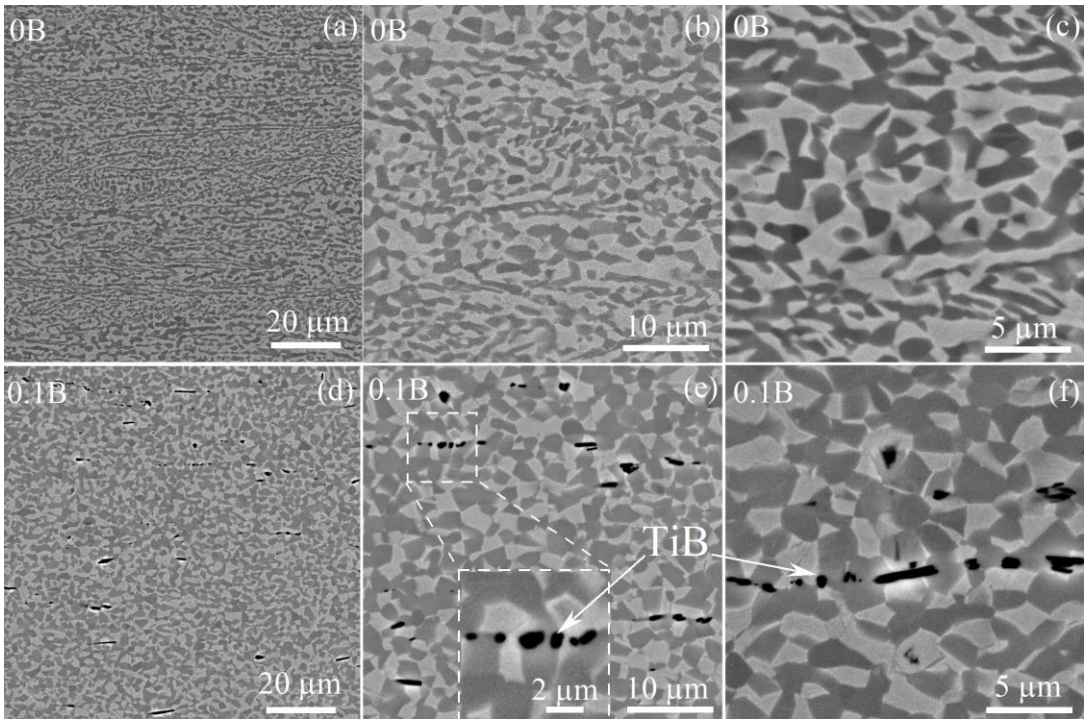

Figure 6. Microstructures of the **(a-c)** 0B and **(d-f)** 0.1B alloys after annealing for 30 min at 875 °C.

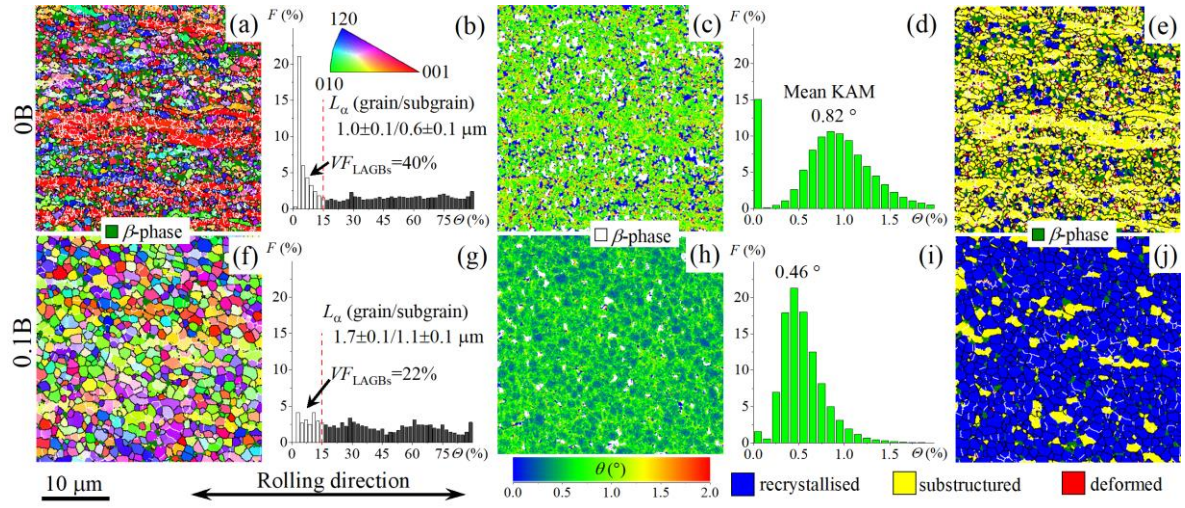

Figure 7. (a,f) EBSD-IPF maps, **(b,g)** the grain boundary misorientation angle distributions, **(c,h)** kernel average misorientation (KAM) maps, **(d,i)** the local misorientation distributions and **(e,j)** recrystallized fraction map of the **(a-e)** 0B and **(f-j)** 0.1B alloys after annealing for 30 min at 875 °C.

3.4. Superplastic deformation

Alloys with 0.01-0.1%B similar to the reference B-free alloy exhibited superplasticity at 875 °C with a strain rate sensitivity coefficient m ~0.5 in a strain rate range of 5×10^{-4} to 5×10^{-3} s^{-1}. Elongation to failure of ~1000% was received at a constant strain rate of 1×10^{-3} s^{-1} (Figures 8,9). At the lower deformation temperature of 775 °C, the maximum m shifted to the lower strain rates of $(2\text{-}4)\times10^{-4}$ s^{-1}, and elongation to failure decreased to 500-600%. At a temperature of 700 °C, the deformation was characterized by a lower coefficient of m ~0.4 and elongations of 400-500%. The elongation to failure insignificantly depended at 875 °C and slightly increases at 700-775 °C due to the trace boron addition of 0.01-0.1%. Moreover, alloys with minor boron addition exhibited significantly smaller flow stresses at the initial stage of deformation than that of the B-free alloy. The differences

Preprints (www.preprints.org) | NOT PEER-REVIEWED | Posted: 11 April 2023 doi:10.20944/preprints202304.0194.v1

in the deformation behavior of the alloys are most pronounced at a temperature of 775 °C. At the initial stage (in a range of ε=0.1-0.7), the deformation of B-free alloy was accompanied by strain softening but a steady flow was observed for the alloys with 0.01-0.1% B (Figure 8e).

Alloys with 1 and 2% B were characterized by lower values of the strain rate sensitivity coefficient *m* than alloys with 0.01-0.1%B at 875 °C; the maximum *m*-value was 0.42 at 1×10^{-3} s^{-1} for the 1B alloy and 0.35 at 2×10^{-4} s^{-1} for the 2B alloy (Figure 8c). The 1B alloy demonstrated the superplastic behavior at the deformation with the strain rate corresponding to the maximum *m*, with elongation to failure of ~500%. The 2B alloy demonstrated non-superplastic behavior even at a low strain rate of 2×10^{-4} s^{-1}; the flow stress for the 2B alloy was higher than for the 1B alloy and the elongation was twice smaller (250%).

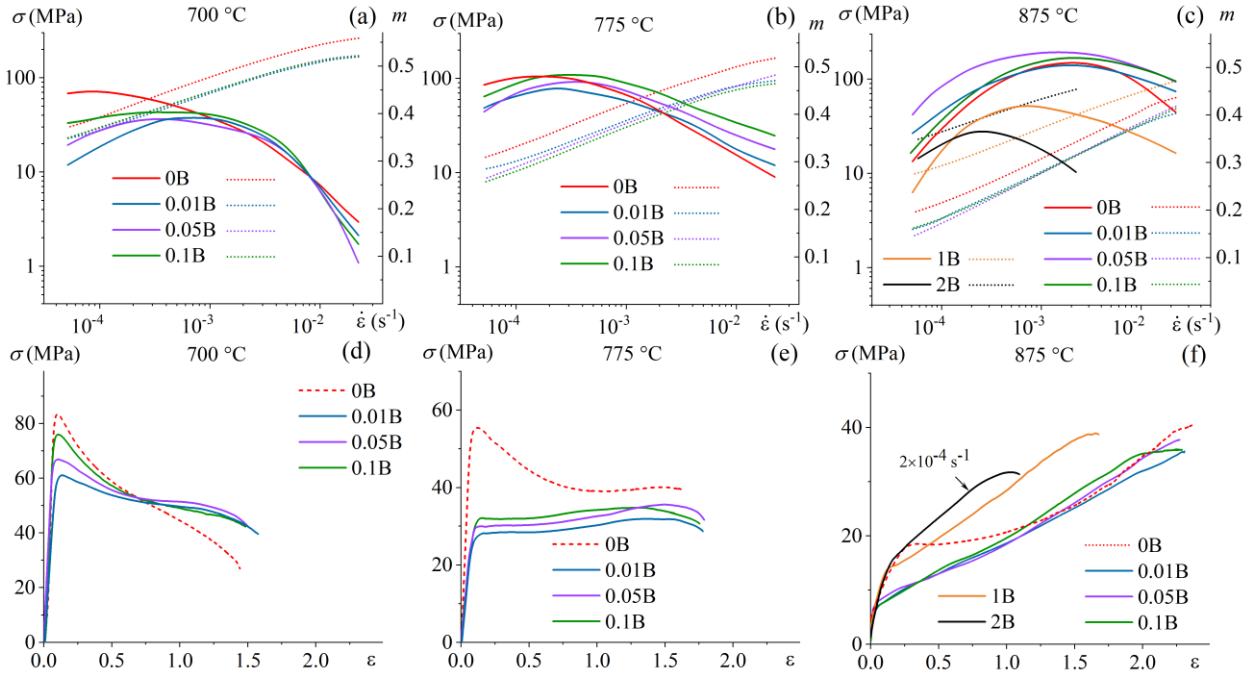

Figure 8. (a-c) Stress vs. strain rate and *m* value vs. strain rate obtained by a step-by-step decrease in the strain rate and **(d–f)** stress–strain curves at a constant strain rate of 1×10^{-3} s^{-1} at **(a,d)** 700 °C, **(b,c)** 825 °C and **(c,f)** 875 °C.

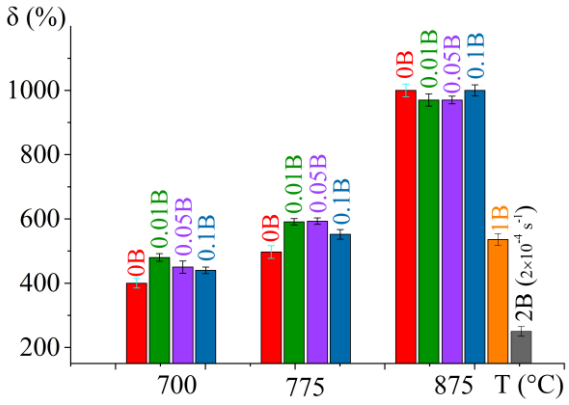

Figure 9. Elongation to failure (δ) dependency in a temperature range of 775-875 °C of the investigated alloys.

Preprints (www.preprints.org) | NOT PEER-REVIEWED | Posted: 11 April 2023 doi:10.20944/preprints202304.0194.v1

3.5. Mechanical Properties

The mechanical properties at room temperature of the alloys studied (yield strength *YS*, ultimate tensile strength *UTS*, and elongation to fracture δ) were determined after deformation at a temperature of 875 °C with a constant strain rate of 1×10^{-3} s^{-1} (2×10^{-4} s^{-1} for the 2B alloy) for a strain of 0.69 (100% of engineering strain) (Table 4). Increasing the boron content decreased the yield strength from 770 MPa for B-free alloy to 680 MPa for 0.1%. The boron in a range of 0.01 to 0.1% insignificantly influenced the UTS and elongation at fracture values, which were 840-870 MPa and 6-7 %, respectively. Increasing boron to 1%B improves both strength characteristics YS to 830 MPa and UTS to 1020 MPa, but drastically dropped ductility to a critically low value of elongation to fracture of ~1 %. Alloy with 2%B demonstrated a brittle fracture and resulted in smaller strength properties. Quenching and aging of the alloys with a low boron content of 0.01-0.1% increased yield strength by 100-130 MPa and tensile strength by 90-140 MPa and insignificantly influenced the elongation at fracture.

Table 4. Room-temperature mechanical properties of the investigated alloys after superplastic deformation.

Alloy	*YS* (MPa)	UTS (MPa)	δ (%)
100 pct strain at 875 °C / 1×10^{-3} s^{-1} and air cooling			
0B	770 ± 10	860 ± 10	7 ± 1
0.01B	733 ± 7	840 ± 10	6 ± 1
0.05B	678 ± 8	840 ± 10	7 ± 1
0.1B	680 ± 7	870 ± 5	7 ± 1
1B	830 ± 8	1020 ± 6	1.1 ± 0.4
2B	-	778 ± 5	-
100 pct strain at 875 °C / 1×10^{-3} s^{-1}, water cooling and ageing at 480 °C for 16 h			
0.01B	865 ± 7	982± 8	7 ± 1
0.1B	780 ± 7	960 ± 5	5 ± 1

4. Discussion

A trace boron addition, up to 0.1%, provided an effective refinement of the prior β grains. A mean grain size decreased more than three times. The grain refinement effect of 0.02-0.2% boron is well known for unalloyed Ti [41], several Ti-based alloys [16,42], and Ti-Ni [43,44] and Ti-Al [45–47] intermetallic alloys. The difference in the grain size between 0.1 and 0.4 wt.% B was insignificant. The boron at the same content of ~0.1% was effective for the grain refinement in the studied Ti-Al-Mo-V alloy. The mechanisms of the B effect for as-cast grain refinement are attributed to the formation of boride particles, which can inhibit grain growth in a β phase field [16,48] or B segregations at the front of solidification due to its extra-low solubility in Ti and distribution coefficient <1 [48,49]. In addition, increasing boron content leads to a decrease in the liquidus temperature of the alloys and a narrowing of the solidification range (Figure 1). This effect should increase the crystallization rate and stimulate nucleation kinetics. A similar grain refinement effect with increasing alloying element content was observed for Al-Mg alloys [50] and Ni-Cu alloys [51]. For the studied hypoeutectic alloys, it was demonstrated that the grain refinement effect disappeared at high boron content of 1-2% B. The mechanism of the phenomenon is unclear. With an increase in boron content from 0.1 to 1-2% the fraction of TiB particles significantly increased and, considering the similar mean size of the boride particles, the Zener pinning effect [25] during cooling in a β-phase field should be stronger and finer grains should be formed. Meanwhile, grains were coarser at a high borides fraction. Similarly, the effect of segregation of boron at the periphery of β dendrites during their growth in a liquid phase should be stronger at higher B content. The microstructure

 doi:10.20944/preprints202304.0194.v1

and boride morphology suggested the same origin of the TiB phase precipitation via eutectic transformation for 0.1%B and 1-2%B. A similar B concentration in eutectic point is observed for Ti-B alloys [30] and slightly smaller ~1.6%B for Ti-6Al-4V-B alloys [32]. The solidification range decreases with the increase of boron from 0.1 to 2% and became narrow for the eutectic concentration of ~2%B. Thus, the nature of the degradation of grain refinement effect for high-boron hypoeutectic alloys is unclear and requires explanations and further investigations. The observed phenomenon also suggests that further clarification of the grain refinement mechanism for prior β-grains via trace boron additions is required. The possible explanation is as follows. First, considering the widely acceptable constitutional supercooling effect, trace boron addition refines the β-phase dendrites, and the change of the crystal growth type from dendritic to eutectic bicrystal with colonies of two phases eliminates this effect. At a high boron content and a high fraction of β phase of eutectic origin, the effect disappeared due to extra-rapid simultaneous growth of TiB and β colonies. At minor concentrations, boron atoms in the liquid may stimulate the nucleation of the β phase due to a decrease of the liquid–solid interphase energy or a decrease in the critical size of nuclei due to B atomic segregations [16,42]. A segregation effect is the most pronounced at the minor content of alloying element or impurity and the distribution of the elements became more homogeneous at its high content [16]. Second, the widely accepted theory for grain refinement during solidification for various alloys is still the inoculation effect, e.g. Ti with B in Al [52], Zr in Mg, or Al [53]. This mechanism seems impossible for hypoeutectic Ti-B alloys when β-phase grains are solidified before the eutectic-originated TiB phase [54]. Meanwhile, the ingots of the studied alloys were re-melted five times, and for low-boron alloys with a high liquidus temperature, high-temperature borides may incompletely dissolute during the re-melting process and provide a heterogeneous nucleation effect. This effect has been noted in [23] as Larson's theory. At a high fraction of Ti+TiB eutectic, TiB colonies rapidly dissolute due to a short-range diffusion and narrow solidification range, smaller liquidus temperature with a higher overheating degree. Third, for low-boron alloys, the precipitation of primary B-induced metastable phases due to non-equilibria solidification or other unconsidered phases with interstitial impurities in a liquid phase may provide heterogeneous nucleation of the β-phase during solidification of the studied alloy. Even a small fraction of such phases is enough to stimulate inoculation. The formation of the thermodynamically stable borides simplifies in the high-boron 1B and 2B alloys and no inoculation effect was observed.

Trace boron alloying also significantly changed the as-annealed microstructure of the thermomechanical processed alloys. The B-free alloy demonstrated an inhomogeneous structure with elongated and equiaxed grains and a high fraction of LAGBs. Alloying with 0.1%B provided a globular microstructure in the alloy and twice decreased LAGB fraction. A similar effect was found due to alloying of Ti-Al-Mo-V alloy by both Fe and B [39]. Thus, boron plays a key role in the acceleration of the recrystallization and further globularization of the grains. These results are consistent with [55] indicating that TiB particles accelerate the microstructure globularization due to particle stimulation nucleation of the α phase [56]. The B atomic segregations at the α/β interfaces, which were recently found in [16], also may facilitate recrystallization and globularization of the microstructure during annealing. As the result, the reference 0B alloy, which was similar to conventional Ti-4Al-1V-3Mo alloy [36,38], exhibited higher flow stress and a stronger softening than alloys with 0.01-0.1% B. The formation of equiaxed grains with high-angle grain or interphase boundaries at the initial stage of deformation facilitated grain boundary sliding and decreased flow stress during superplastic deformation [57]. The boron influence on the deformation behavior was significant at a low deformation temperature of 775 °C (Figure 8 d,e). Thus, alloying with trace boron is an effective strategy to improve the superplasticity of Ti-based alloys at low temperatures, which is of high practical importance for the superplastic forming process. Along with this, the trace B addition decreased the post-forming yield strength of the alloys owing to a higher recrystallized fraction and larger mean grain size than B-free alloy.

 doi:10.20944/preprints202304.0194.v1

Due to a high fraction of borides, an increase in B content to 1% increases room temperature strength but weakens superplastic properties and decreases ductility at both elevated and room temperatures. The same influence of boron on the room temperature properties was observed for Ti-6Al-4V alloy [58]. Authors of [15,59] observed an increased strength but decreased ductility and fracture toughness for the alloys with 0.4-2%B. To increase ductility and toughness the morphology of borides should be changed from whiskers to spherical shapes. Notably, that thermo-mechanical treatment of the alloy with 2%B provided refinement of TiB particles during high-temperature deformation and contributed to the formation of more compact particles. Particle refinement may be the result of both mechanical breaking [60,61] and fragmentation and spheroidization processes during hot deformation at an elevated temperature of 900 °C. The same processes occur during the spheroidization of cementite in steel [62,63] or intermetallic particles in aluminum-based alloys [64,65]. Despite the size of about 1 μm, the TiB particles induced a drop in ductility and led to an embrittlement effect in 2%B alloy. Meanwhile, the alloy with 1%B demonstrated an acceptable combination of high-temperature superplasticity at 875 °C and a high room-temperature tensile strength. To avoid embrittlement, the high boron alloys alloy the sheet processing technologies should be focused on the morphology of borides.

5. Conclusions

The influence of 0.01-2%B on the microstructure, superplasticity, and mechanical properties at room temperature of the Ti-4%Al-3%Mo-1%V alloy was studied. The boron effect on the microstructure and properties of the alloy was strongly different for the ranges of 0.01-0.1%B and 1-2%B. The main conclusions are summarized as follows.

The TiB particles of eutectic origin were formed after solidification. In as-cast alloys, the mean size of borides increased from 0.7 to 2.5 μm with an increase B from 0.01 to 0.1% and insignificantly changed in a range of 0.1-2% B. The volume fraction of the TiB phase increased from 0.1% at 0.01 wt.%B to 10.8% at 2 wt.% B that agreed to Thermo Calc simulation. Trace boron addition significantly reduced the mean size of prior β grains from ~700 μm in B-free alloy to ~210 μm for the alloy with 0.1%B. Grain refinement was not revealed and a mean grain size was ~670-750 μm at a B content of 1-2 wt.%.

After thermomechanical treatment with a final hot rolling, the alloys exhibited a similar microstructure with elongated grains of the α and β phases and differ by TiB particle size and volume fraction. The whisker-shaped particles have a thickness of ~0.6-0.7 μm and a length of ~2-3 μm at 0.01-1 wt.% B and an equiaxed shape TiB particles with a size of ~1 μm were observed at 2 wt.% B.

Elevated temperature annealing led to a non-uniform structure with a high fraction of high-angle grain boundaries for B-free alloy and a globular recrystallized structure for the alloy with 0.1 wt.% B. Due to the facilitation of recrystallization and globularization effects, the 0.01-0.1 wt.% B decreased flow stress values at the initial stage of deformation. The effect was significant at a low deformation temperature of 775 °C. The strain rate sensitivity coefficient m was ~0.5, and the elongation to failure was ~500-1000% during superplastic deformation at temperatures of 775-875 °C with a strain rate of 1×10^{-3} s^{-1}. Along with this, at room temperature the elongation to fracture was 7% for all studied alloys but, owing to a recrystallized structure, post-forming tensile yield strength decreased from 770 MPa for the B-free alloy to 680 MPa for the alloy with 0.1 wt% B. Quenching and aging increased the strength properties of 90-140 MPa.

Alloy with 1 wt% B exhibits the superplastic behavior with m of 0.5 and elongation to failure of ~500% at 875 °C and room temperature yield strength of 830 MPa, ultimate strength of 1020 MPa, and low elongation of 1.1%. Eutectic alloy with 2 wt% B demonstrated a brittle fracture and a strong weakening of strength, ultimate tensile strength decreased to 780 MPa.

Author Contributions: Methodology, data curation, and investigation, M.N.P. and A.I.B; visualization and formal analysis, A.O.M. and S.V.M.; conceptualization, supervision, writing, review and editing, A.D.K. and A.V.M. All authors have read and agreed to the published version of the manuscript.

Funding: The study of alloys with small additions of boron of 0.01-0.1% was funded by the Russian Science Foundation (Grant #21-79-10380).

Institutional Review Board Statement: Not applicable.

Informed Consent Statement: Not applicable.
Data Availability Statement: Not applicable.

Acknowledgments: In this section, you can acknowledge any support given which is not covered by the author contribution or funding sections. This may include administrative and technical support, or donations in kind (e.g., materials used for experiments).

Conflicts of Interest: The authors declare no conflict of interest.

References

1. Moiseyev, V.N. *Titanium Alloys: Russian Aircraft and Aerospace Applications*; CRC Press: Boca Raton, FL, USA, 2005; ISBN 9780849332739.
2. Ridley, N. Metals for Superplastic Forming. *Superplast. Form. Adv. Met. Mater. Methods Appl.* **2011**, 3–33, doi:10.1016/B978-1-84569-753-2.50001-7.
3. Novikov, I.I.; Portnoj, V.K. *Superplastizität von Legierungen*; VEB Deutscher Verlag fur Grundstoffindustrie. Leipzig, Ed.; 1985;
4. Meier, M.L.; Lesuer, D.R.; Mukherjee, A.K. *A Grain Size and Fl Volume Fraction Aspects of the Superplasticity of Ti-6A1-4V*; 1991; Vol. 136;.
5. Sieniawski, J.; Motyka, M. Superplasticity in Titanium Alloys. *Jounal Achiev. Mater. Manuf. Eng.* **2007**.
6. Sinha, V.; Srinivasan, R.; Tamirisakandala, S.; Miracle, D.B. Superplastic Behavior of Ti-6Al-4V-0.1B Alloy. *Mater. Sci. Eng. A* **2012**, *539*, 7–12, doi:10.1016/j.msea.2011.12.058.
7. Roy, S.; Suwas, S. Deformation Mechanisms during Superplastic Testing of Ti-6Al-4V-0.1B Alloy. *Mater. Sci. Eng. A* **2013**, *574*, 205–217, doi:10.1016/j.msea.2013.03.013.
8. Imayev, V.M.; Gaisin, R.A.; Imayev, R.M. Effect of Boron Addition on Formation of a Fine-Grained Microstructure in Commercially Pure Titanium Processed by Hot Compression. *Mater. Sci. Eng. A* **2015**, *639*, 691–698, doi:10.1016/j.msea.2015.05.082.
9. Roy, S.; Suwas, S.; Tamirisakandala, S.; Miracle, D.B.; Srinivasan, R. Development of Solidification Microstructure in Boron-Modified Alloy Ti-6Al-4V-0.1B. *Acta Mater.* **2011**, doi:10.1016/j.actamat.2011.05.023.
10. Singh, G.; Ramamurty, U. Boron Modified Titanium Alloys. *Prog. Mater. Sci.* **2020**, *111*, 100653, doi:10.1016/j.pmatsci.2020.100653.
11. Palty, A.E.; Margolin, H.; Nielsen, J.P. TITANIUM NITROGEN AND TITANIUM BORON SYSTEMS. *Trans. Am. Soc. Met.* **1954**, *46*, 312–328.
12. Yang, Y.F.; Yan, M.; Luo, S.D.; Schaffer, G.B.; Qian, M. Modification of the α-Ti Laths to near Equiaxed α-Ti Grains in as-Sintered Titanium and Titanium Alloys by a Small Addition of Boron. *J. Alloys Compd.* **2013**, *579*, 553–557, doi:10.1016/j.jallcom.2013.07.097.
13. Nandwana, P.; Nag, S.; Hill, D.; Tiley, J.; Fraser, H.L.; Banerjee, R. On the Correlation between the Morphology of α and Its Crystallographic Orientation Relationship with TiB and β in Boron-Containing Ti-5Al-5Mo-5V-3Cr-0.5Fe Alloy. *Scr. Mater.* **2012**, *66*, 598–601, doi:10.1016/j.scriptamat.2012.01.011.
14. Sasaki, T.T.; Fu, B.; Torres, K.; Thompson, G.B.; Srinivasan, R.; Cherukuri, B.; Tiley, J. Nucleation and Growth of α-Ti on TiB Precipitates in Ti-15Mo-2.6Nb-3Al-0.2Si-0.12B. *Philos. Mag.* **2011**, *91*, 850–864, doi:10.1080/14786435.2010.533134.
15. SEN, I.; TAMIRISAKANDALA, S.; MIRACLE, D.; RAMAMURTY, U. Microstructural Effects on the Mechanical Behavior of B-Modified Ti–6Al–4V Alloys. *Acta Mater.* **2007**, *55*, 4983–4993, doi:10.1016/j.actamat.2007.05.009.

16. Chong, Y.; Gholizadeh, R.; Yamamoto, K.; Tsuji, N. New Insights into the Colony Refinement Mechanism by Solute Boron Atoms in Ti-6Al-4V Alloy. *Scr. Mater.* **2023**, *230*, 115397, doi:10.1016/j.scriptamat.2023.115397.
17. Roy, S.; Suwas, S. The Influence of Temperature and Strain Rate on the Deformation Response and Microstructural Evolution during Hot Compression of a Titanium Alloy Ti–6Al–4V–0.1B. *J. Alloys Compd.* **2013**, *548*, 110–125, doi:10.1016/j.jallcom.2012.08.123.
18. Gaisin, R.A.; Imayev, V.M.; Imayev, R.M.; Gaisina, E.R. Effect of Boron Addition on Recrystallization Behavior of Commercially Pure Titanium Subjected to Hot Compression. *Lett. Mater.* **2015**, *5*, 124–128, doi:10.22226/2410-3535-2015-2-124-128.
19. Srinivasan, R.; Miracle, D.; Tamirisakandala, S. Direct Rolling of As-Cast Ti-6Al-4V Modified with Trace Additions of Boron. *Mater. Sci. Eng. A* **2008**, *487*, 541–551, doi:10.1016/j.msea.2007.10.053.
20. Roy, S.; Sarkar, A.; Suwas, S. On Characterization of Deformation Microstructure in Boron Modified Ti-6Al-4V Alloy. *Mater. Sci. Eng. A* **2010**, *528*, 449–458, doi:10.1016/j.msea.2010.09.026.
21. Gaisin, R.A.; Imayev, V.M.; Imayev, R.M.; Gaisina, E.R. Microstructure and Hot Deformation Behavior of Two-Phase Boron-Modified Titanium Alloy VT8. *Phys. Met. Metallogr.* **2013**, *114*, 339–347, doi:10.1134/S0031918X13040042.
22. Stefanescu, D.M.; Ruxanda, R. Solidification Structures of Titanium Alloys. In *Metallography and Microstructures*; ASM International, 2004; pp. 116–126.
23. Cheng, T.. The Mechanism of Grain Refinement in TiAl Alloys by Boron Addition — an Alternative Hypothesis. *Intermetallics* **2000**, *8*, 29–37, doi:10.1016/S0966-9795(99)00063-1.
24. Tamirisakandala, S.; Bhat, R.B.; Tiley, J.S.; Miracle, D.B. Grain Refinement of Cast Titanium Alloys via Trace Boron Addition. *Scr. Mater.* **2005**, *53*, 1421–1426, doi:10.1016/j.scriptamat.2005.08.020.
25. CHERUKURI, B.; SRINIVASAN, R.; TAMIRISAKANDALA, S.; MIRACLE, D. The Influence of Trace Boron Addition on Grain Growth Kinetics of the Beta Phase in the Beta Titanium Alloy Ti–15Mo–2.6Nb–3Al–0.2Si. *Scr. Mater.* **2009**, *60*, 496–499, doi:10.1016/j.scriptamat.2008.11.040.
26. Bilous, O.O.; Artyukh, L.V.; Bondar, A.A.; Velikanova, T.Y.; Burka, M.P.; Brodnikovskyi, M.P.; Fomichov, O.S.; Tsyganenko, N.I.; Firstov, S.O. Effect of Boron on the Structure and Mechanical Properties of Ti–6Al and Ti–6Al–4V. *Mater. Sci. Eng. A* **2005**, *402*, 76–83, doi:10.1016/j.msea.2005.05.011.
27. Luan, J.H.; Jiao, Z.B.; Chen, G.; Liu, C.T. Improved Ductility and Oxidation Resistance of Cast Ti–6Al–4V Alloys by Microalloying. *J. Alloys Compd.* **2014**, *602*, 235–240, doi:10.1016/j.jallcom.2014.03.039.
28. Roy, S.; Suwas, S. Enhanced Superplasticity for (A+β)-Hot Rolled Ti-6Al-4V-0.1B Alloy by Means of Dynamic Globularization. *Mater. Des.* **2014**, doi:10.1016/j.matdes.2014.01.033.
29. Kotov, A.D.; Postnikova, M.N.; Mosleh, A.O.; Mikhaylovskaya, A. V. Influence of Fe on the Microstructure, Superplasticity and Room-Temperature Mechanical Properties of Ti–4Al–3Mo–1V-0.1B Alloy. *Mater. Sci. Eng. A* **2022**, *845*, 143245, doi:10.1016/j.msea.2022.143245.
30. Tamirisakandaia, S.; Miracle, D.B.; Srinivasan, R.; Gunasekera, J.S. Titanium Alloyed with Boron. *Adv. Mater. Process.* **2006**, *164*, 41–43.
31. Hill, D.; Banerjee, R.; Huber, D.; Tiley, J.; Fraser, H.L. Formation of Equiaxed Alpha in TiB Reinforced Ti Alloy Composites. *Scr. Mater.* **2005**, *52*, 387–392, doi:10.1016/j.scriptamat.2004.10.019.
32. Ivasishin, O.M.; Teliovych, R. V.; Ivanchenko, V.G.; Tamirisakandala, S.; Miracle, D.B. Processing, Microstructure, Texture, and Tensile Properties of the Ti-6Al-4V-1.55B Eutectic Alloy. *Metall. Mater. Trans. A* **2008**, *39*, 402–416, doi:10.1007/s11661-007-9425-x.
33. Roy, S.; Suwas, S. Deformation Mechanisms during Superplastic Testing of Ti-6Al-4V-0.1B Alloy. *Mater. Sci. Eng. A* **2013**, doi:10.1016/j.msea.2013.03.013.
34. Zadorozhnyy, V.Y.; Shchetinin, I.V.; Chirikov, N.V.; Louzguine-Luzgin, D.V. Tensile Properties of a Dual-Axial Forged Ti–Fe–Cu Alloy Containing Boron. *Mater. Sci. Eng. A* **2014**, *614*, 238–242, doi:10.1016/j.msea.2014.07.017.

35. Chandravanshi, V.K.; Sarkar, R.; Kamat, S. V.; Nandy, T.K. Effect of Boron on Microstructure and Mechanical Properties of Thermomechanically Processed near Alpha Titanium Alloy Ti-1100. *J. Alloys Compd.* **2011**, *509*, 5506–5514, doi:10.1016/j.jallcom.2011.02.114.
36. Kotov, A.D.; Mikhailovskaya, A. V.; Mosleh, A.O.; Pourcelot, T.P.; Prosviryakov, A.S.; Portnoi, V.K. Superplasticity of an Ultrafine-Grained Ti–4% Al–1% V–3% Mo Alloy. *Phys. Met. Metallogr.* **2019**, *120*, 60–68, doi:10.1134/S0031918X18100083.
37. Mosleh, A.O.; Mikhaylovskaya, A. V; Kotov, A.D.; Sitkina, M.; Mestre-Rinn, P.; Kwame, J.S. Superplastic Deformation Behavior of Ultra-Fine-Grained Ti-1V-4Al-3Mo Alloy: Constitutive Modeling and Processing Map. *Mater. Res. Express* **2019**, doi:10.1088/2053-1591/ab31f9.
38. Mosleh, A.O.; Kotov, A.D.; Vidal, V.; Mochugovskiy, A.G.; Velay, V.; Mikhaylovskaya, A.V. Initial Microstructure Influence on Ti–Al–Mo–V Alloy's Superplastic Deformation Behavior and Deformation Mechanisms. *Mater. Sci. Eng. A* **2021**, *802*, 140626, doi:10.1016/j.msea.2020.140626.
39. Mikhaylovskaya, A. V.; Mosleh, A.O.; Mestre-Rinn, P.; Kotov, A.D.; Sitkina, M.N.; Bazlov, A.I.; Louzguine-Luzgin, D. V. High-Strength Titanium-Based Alloy for Low-Temperature Superplastic Forming. *Metall. Mater. Trans. A Phys. Metall. Mater. Sci.* **2021**, *52*, 293–302, doi:10.1007/s11661-020-06058-8.
40. Kotov, A.D.; Postnikova, M.N.; Mosleh, A.O.; Mikhaylovskaya, A. V. Influence of Fe on the Microstructure, Superplasticity and Room-Temperature Mechanical Properties of Ti–4Al–3Mo–1V-0.1B Alloy. *Mater. Sci. Eng. A* **2022**, *845*, 143245, doi:10.1016/j.msea.2022.143245.
41. Imayev, V.M.; Gaisin, R.A.; Imayev, R.M. Effect of Boron Addition on Formation of a Fine-Grained Microstructure in Commercially Pure Titanium Processed by Hot Compression. *Mater. Sci. Eng. A* **2015**, *639*, 691–698, doi:10.1016/j.msea.2015.05.082.
42. Tamirisakandala, S.; Bhat, R.B.; Tiley, J.S.; Miracle, D.B. Grain Refinement of Cast Titanium Alloys via Trace Boron Addition. *Scr. Mater.* **2005**, *53*, 1421–1426, doi:10.1016/j.scriptamat.2005.08.020.
43. Suzuki, Y.; Xu, Y.; Morito, S.; Otsuka, K.; Mitose, K. Effects of Boron Addition on Microstructure and Mechanical Properties of Ti–Td–Ni High-Temperature Shape Memory Alloys. *Mater. Lett.* **1998**, *36*, 85–94, doi:10.1016/S0167-577X(98)00009-3.
44. YEN, F.-C.; HWANG, K.-C. Microstructures, Mechanical Properties, and Shape Memory Characteristics of Powder Metallurgy Ti51Ni49 Modified with Boron. *Metall. Mater. Trans. A* **2012**, *43*, 687–696, doi:10.1007/s11661-011-0894-6.
45. Liu, C.T.; Schneibel, J.H.; Maziasz, P.J.; Wright, J.L.; Easton, D.S. Tensile Properties and Fracture Toughness of TiAl Alloys with Controlled Microstructures. *Intermetallics* **1996**, *4*, 429–440, doi:10.1016/0966-9795(96)00047-7.
46. Christodoulou, J.A.; Flower, H.M. The Role of Borides in Near-γ Titanium Aluminides. *Adv. Eng. Mater.* **2000**, *2*, 631–638, doi:10.1002/1527-2648(200010)2:10<631::AID-ADEM631>3.0.CO;2-5.
47. Hu, D. A Quarter Century Journey of Boron as a Grain Refiner in TiAl Alloys. *TMS Annu. Meet.* **2014**, *2014-Febru*, 21–30, doi:10.1002/9781118998489.ch3.
48. Bermingham, M.J.; McDonald, S.D.; Nogita, K.; St. John, D.H.; Dargusch, M.S. Effects of Boron on Microstructure in Cast Titanium Alloys. *Scr. Mater.* **2008**, *59*, 538–541, doi:10.1016/j.scriptamat.2008.05.002.
49. Tamirisakandala, S.; Bhat, R.B.; Miracle, D.B.; Boddapati, S.; Bordia, R.; Vanover, R.; Vasudevan, V.K. Effect of Boron on the Beta Transus of Ti-6Al-4V Alloy. *Scr. Mater.* **2005**, *53*, 217–222, doi:10.1016/j.scriptamat.2005.03.038.
50. Kishchik, A.A.; Mikhaylovskaya, A. V.; Levchenko, V.S.; Portnoy, V.K. Formation of Microstructure and the Superplasticity of Al–Mg-Based Alloys. *Phys. Met. Metallogr.* **2017**, *118*, 96–103, doi:10.1134/S0031918X16120085.
51. Tarshis, L.A.; Walker, J.L.; Rutter, J.W. Experiments on the Solidification Structure of Alloy Castings. *Metall. Trans.* **1971**, *2*, 2589–2597, doi:10.1007/BF02814899.
52. Gan, G.; Yang, B.; Zhang, B.; Jiang, X.; Shi, Y.; Wu, Y. Refining Mechanism of 7075 Al Alloy by In-Situ TiB2 Particles. *Materials (Basel).* **2017**, *10*, 1–11, doi:10.3390/ma10020132.
53. Sun, M.; Yang, D.; Zhang, Y.; Mao, L.; Li, X.; Pang, S. Recent Advances in the Grain Refinement Effects of Zr on Mg Alloys: A Review. *Metals (Basel).* **2022**, *12*, doi:10.3390/met12081388.

54. Okamoto, H.; Massalski, T.B. Section I: Basic and Applied Research Binary Alloy Phase Diagrams. **1994**, *15*, 500–521.
55. Anil Kumar, V.; Murty, S.V.S.N.; Gupta, R.K.; Rao, A.G.; Prasad, M.J.N.V. Effect of Boron on Microstructure Evolution and Hot Tensile Deformation Behavior of Ti-5Al-5V-5Mo-1Cr-1Fe Alloy. *J. Alloys Compd.* **2020**, *831*, 154672, doi:10.1016/j.jallcom.2020.154672.
56. Hill, D.; Banerjee, R.; Huber, D.; Tiley, J.; Fraser, H.L. Formation of Equiaxed Alpha in TiB Reinforced Ti Alloy Composites. *Scr. Mater.* **2005**, *52*, 387–392, doi:10.1016/j.scriptamat.2004.10.019.
57. Nieh, T.G.; Wadsworth, J.; Sherby, O.D. *Superplasticity in Metals and Ceramics*; Cambridge University Press, 1997; ISBN 9780521561051.
58. Yutao Zhai, P.S.; Bolzoni, L.; Qu, Y. Fabrication and Characterization of In Situ Ti-6Al-4V / TiB. *Metals (Basel).* **2022**.
59. Zhu, J.; Kamiya, A.; Yamada, T.; Shi, W.; Naganuma, K. Influence of Boron Addition on Microstructure and Mechanical Properties of Dental Cast Titanium Alloys. *Mater. Sci. Eng. A* **2003**, *339*, 53–62, doi:10.1016/S0921-5093(02)00102-8.
60. Zherebtsov, S.; Ozerov, M.; Klimova, M.; Stepanov, N.; Vershinina, T.; Ivanisenko, Y.; Salishchev, G. Effect of High-Pressure Torsion on Structure and Properties of Ti-15Mo/TiB Metal-Matrix Composite. *Materials (Basel).* **2018**, *11*, 2426, doi:10.3390/ma11122426.
61. Markovsky, P.E.; Janiszewski, J.; Stasyuk, O.O.; Bondarchuk, V.I.; Savvakin, D.G.; Cieplak, K.; Goran, D.; Soni, P.; Prikhodko, S. V. Mechanical Behavior of Titanium Based Metal Matrix Composites Reinforced with TiC or TiB Particles under Quasi-Static and High Strain-Rate Compression. *Materials (Basel).* **2021**, *14*, 6837, doi:10.3390/ma14226837.
62. Zhou, L.; Liu, G.; Ma, X.L.; Lu, K. Strain-Induced Refinement in a Steel with Spheroidal Cementite Subjected to Surface Mechanical Attrition Treatment. *Acta Mater.* **2008**, *56*, 78–87, doi:10.1016/j.actamat.2007.09.003.
63. Wu, T.; Wang, M.; Gao, Y.; Li, X.; Zhao, Y.; Zou, Q. Effects of Plastic Warm Deformation on Cementite Spheroidization of a Eutectoid Steel. *J. Iron Steel Res. Int.* **2012**, *19*, 60–66, doi:10.1016/S1006-706X(12)60140-X.
64. Portnoy, V.K.; Rylov, D.S.; Levchenko, V.S.; Mikhaylovskaya, A.V. The Influence of Chromium on the Structure and Superplasticity of Al–Mg–Mn Alloys. *J. Alloys Compd.* **2013**, *581*, 313–317, doi:10.1016/j.jallcom.2013.07.075.
65. Kishchik, A.A.; Kotov, A.D.; Mikhaylovskaya, A. V. The Microstructure and High-Strain-Rate Superplasticity of the Al–Mg–Ni–Fe–Mn–Cr–Zr Alloy. *Phys. Met. Metallogr.* **2019**, *120*, 1006–1013, doi:10.1134/S0031918X19100041.